THE PLASMA PHYSICS OF DILUTE ULTRARELATIVISTIC e^+e^- PAIR BEAMS I: LINEAR THEORY

Avery E. Broderick[1,2], Philip Chang[3], Christoph Pfrommer[4], Ewald Puchwein[5],

[1] Perimeter Institute for Theoretical Physics, 31 Caroline Street North, Waterloo, ON, N2L 2Y5, Canada

[2] Department of Physics and Astronomy, University of Waterloo, 200 University Avenue West, Waterloo, ON, N2L 3G1, Canada

[3] Department of Physics, University of Wisconsin-Milwaukee, 1900 E. Kenwood Boulevard, Milwaukee, WI 53211, USA; chang65@uwm.edu

[4] Heidelberg Institute for Theoretical Studies, Schloss-Wolfsbrunnenweg 35, D-69118 Heidelberg, Germany; christoph.pfrommer@h-its.org

Draft version April 26, 2016

ABSTRACT

The annihilation of TeV photons from extragalactic TeV sources and the extragalactic background light produces ultrarelativistic e^+e^- beams, which are subject to powerful plasma instabilities that sap their kinetic energy. Here we study the initial conditions of these e^+e^- beams and the linear phase of the plasma instabilities that cool them. Starting from an isotropic distribution in the center of mass frame, we show that the velocity dispersions parallel and transverse to the direction of beam propagation become highly anisotropic under Lorentz boosts and scale differently with the Lorentz factor, γ. Using these results to construct a simplified distribution function, we then calculate the linear growth rate of the beam plasma and "oblique" instability in both the reactive and kinetic regimes. We reproduce the well-known reactive growth rates for both the beam plasma and "oblique" mode and show that they both have similar growth rates in the kinetic regime. In contrast to the earlier claim by the authors that the oblique mode is dominant, we instead find that both the beam-plasma (parallel) and oblique modes are similarly strong. In addition, we also delineate the conditions for applicability for the reactive and kinetic regimes and find that the beam plasma mode transitions to the reactive regime at a lower γ than the "oblique" mode due to a combination of their different scalings and the anisotropy of the velocity dispersions. Applying these results to the ultrarelativistic e^+e^- beams from TeV blazars, we not only confirm that these beams are unstable to the kinetic "oblique" mode. For sufficiently cold beams in the beam direction or for sufficiently larger Lorentz factor, these beams are also unstable to the "reactive" beam-plasma instability. We show that overall growth rates for both the "oblique" and beam plasma growth rates are similar and in line with our earlier claims. These results strengthen the case that powerful plasma instabilities sap the energy of the ultrarelativistic e^+e^- beams as they propagate through intergalactic space, which has profound consequences on constraints of the intergalactic magnetic field, the thermal state of the intergalactic medium, and the formation of structure in the universe.

Subject headings: BL Lacertae objects: general – gamma rays: general – plasmas – instabilities – magnetic fields

1. INTRODUCTION

The *Fermi* satellite and ground based imaging atmospheric Cerenkov telescopes such as H.E.S.S., MAGIC, and VERI-TAS[1] have demonstrated that the ultra-high energy Universe is teeming with energetic very high-energy gamma-ray (VHEGR, $E > 100\,\mathrm{GeV}$) sources, the extragalactic component of which mainly consists of TeV blazars with a minority population of other sources such as radio galaxies and starburst galaxies. These VHEGR observations have proven to be useful in constraining mechanisms of particle acceleration (see, e.g., Paglione et al. 1996; Domingo-Santamaría & Torres 2005; Thompson et al. 2007; Persic et al. 2008; de Cea del Pozo et al. 2009; Rephaeli et al. 2010; Lacki et al. 2011) and black hole jets (see, e.g., Jones et al. 1974; Ghisellini & Maraschi 1989; Ghisellini & Tavecchio 2008; Tavecchio & Ghisellini 2008; Ghisellini et al. 2009).

It has recently been argued by a number authors that the *non-observation* of $\sim 1-100\,\mathrm{GeV}$ flux by the *Fermi* satellite toward these TeV blazars provides lower bounds on the strength of the intergalactic magnetic field (IGMF) of $B \gtrsim 10^{-19} - 10^{-15}\,\mathrm{G}$ (Neronov & Vovk 2010; Tavecchio et al. 2010, 2011; Dermer et al. 2011; Taylor et al. 2011; Dolag et al. 2011; Takahashi et al. 2012; Vovk et al. 2012). To understand how these claimed

[1] High Energy Stereoscopic System, Major Atmospheric Gamma Imaging Cerenkov Telescope, Very Energetic Radiation Imaging Telescope Array System.

limits arise, we begin by revisiting the physics of VHEGR propagation in the universe.

As these VHEGR photon propagate through the universe, they pair produce off the extragalactic background light (EBL) and produce ultrarelativistic electron-positron beams with typical Lorentz factors of 10^5–10^7. Within the current epoch, the mean free path for these photons is $D_{\mathrm{pp}} \sim 800\,E_{\mathrm{TeV}}^{-1}\,\mathrm{Mpc}$, where $E_{\mathrm{TeV}} = E/1\,\mathrm{TeV}$ is the energy of the photon in TeV. At high redshifts, $z \geq 1$, this drops to $D_{\mathrm{pp}} \sim 35\,E_{\mathrm{TeV}}^{-1}\,\mathrm{Mpc}$ due to the larger number density of EBL photons. Because these typical mean free paths are much shorter than the Hubble length, the universe is optically thick to VHEGRs. This effect is seen in the relative nearness of TeV blazars ($z \sim 0.1$) and the observed softening of their VHE spectra with increasing distance.

Previously, it has been assumed that the resultant electron-positron pairs lose energy through inverse-Compton scattering the cosmic microwave background (CMB) and EBL. This yields an inverse-Compton cascade (ICC) that reprocesses TeV emission to gamma-rays with energies $\lesssim 100\,\mathrm{GeV}$, for which the mean free path is comparable to the size of the universe. Hence, associated with every VHEGR source should be a $\sim 100\,\mathrm{GeV}$ source. It is the *non-observation* of this 100 GeV flux, presumably due to the magnetic deflection of the pairs, that is used to constraint the strength of a putative IGMF.

In addition, *Fermi* has also provided the most precise estimate of the unresolved extragalactic gamma-ray background (EGRB) for energies between 200 MeV and 100 GeV. Since

ICCs reprocess the VHEGR emission of distant sources into this band, this has been used to constrain the evolution of the luminosity density of VHEGR sources (see, e.g., Narumoto & Totani 2006; Kneiske & Mannheim 2008; Inoue & Totani 2009; Venters 2010). These constraints preclude any dramatic rise in numbers of source by $z \sim 1$–2 that seen in the quasar distribution. That is, the comoving number of blazars must have remained essentially fixed, at odds with both the physical picture underlying these systems and with the observed evolution of similarly accreting systems, i.e., quasars.

Ultimately, these conclusions rest upon the assumption that ICCs dominate the evolution of the ultra-relativistic pairs. However, we have strongly challenged this assumption in a recent series of papers, Broderick et al. (2012); Chang et al. (2012); Pfrommer et al. (2012, hereafter paper I, II, and III respectively). In particular, we find that ultrarelativistic pair beam that results from TeV photon annihilation on the EBL is subject to virulent plasma beam instabilities that sap the energy of the pair beam and convert it to heat in the intergalactic medium (IGM) before ICCs have a chance to act.

In Paper I, we showed that despite the extraordinarily dilute nature of this ultra-relativistic pair plasma, a variety of plasma instabilities grow on timescales short in comparison to the inverse-Compton cooling time. Of the three instabilities that we studied — the beam-plasma or two-stream instability[2], the Weibel instability, and the "oblique" instability — the most important of which is the "oblique" instability (Bret et al. 2004) Because the pairs lose their energy primarily via depositing it as heat into the IGM, the ICCs critical to the above arguments commonly employed to provide constraints upon the IGMF and high-redshift blazar population are necessarily precluded. In the latter case in particular, the *Fermi* limits on the EGRB and high-energy blazar statistics allow a large and evolving blazar population more similar to that found for other AGN.

Assuming that these plasma-instability mechanisms drive ultra-relativistic pairs to deposit their energy as heat in the IGM, we explored the impact of this heating on the thermodynamics of the IGM in Paper II and the effect on this additional heating on structure formation in the universe in Paper III. By correcting for the selection effects of the current pencil beam VHEGR observations using the all-sky monitoring of the *Fermi* satellite, we argued that luminosity density in VHE-GRs is of order 0.2% of the quasar luminosity density in Paper II. Because of the greater conversion efficiency of TeV photon energy to heat (as compared to photoheating), we showed that this heating dominates the photoheating rate at low z. This steady volumetric homogeneous heating naturally produces an inverted temperature-density relation and, with only a minor rescaling of the empirically determined TeV blazar heating normalization, reproduces the inferred inverted temperature-density relation at $z = 2 - 3$ (Bolton & Becker 2009; Viel et al. 2009), a feature that standard reionization models have proven unable to reproduce (McQuinn et al. 2009; Bolton & Becker 2009).

Following the work of Paper II, we studied the effects of blazar heating in a more detailed hydrodynamic model of structure formation (Puchwein et al. 2012). Using the same blazar heating prescription as in Paper II, we showed that the optical depth of the Lyα forest is reproduced using a H I pho-

toionization rate of $\Gamma_{\mathrm{HI}} \approx 5 \times 10^{-13}\,\mathrm{s}^{-1}$ or equivalently using the inferred ionizing background from Faucher-Giguère et al. (2009). We also demonstrated that the low-density IGM again possesses an inverted temperature-density relation, confirming the results of Paper II in greater detail. In addition, we showed that a blazar heated universe not only matches the one- and two-point statistics of the high redshift Lyα forest but also the linewidth and column depth distribution. This excellent quantitative agreement is achieved without tuning the photoionizing background and is due specifically to the excess energy injection into the low-density IGM from TeV blazars.

Finally in Paper III, we explored the result of this additional IGM heating upon the formation of structure in the Universe. In particular, we showed that the injection of entropy into the IGM by TeV blazars contributes to developing a redshift dependent entropy floor for galaxy clusters and groups at $z \lesssim 2$ and suppresses the formation of dwarfs. The redshift dependent nature of TeV blazar heating suggests a large injection of entropy around $z \sim 1$, boosting the entropy of late forming groups and clusters. This predicted enhanced entropy of young groups is consistent with recent observations that show optically bright, and therefore young, groups and clusters are X-ray dim — that is having a lower gas density due to a raised entropy floor. We also found that TeV blazar heating suppresses the formation of late forming dwarfs both in galactic halos, which is potentially important for the missing satellite problem (Kravtsov 2010), and in voids, which is likewise potentially important for the void phenomenon (Peebles 2001), by raising the temperature of the IGM such that gas cannot collapse to form galaxies.

These potential implications of blazar heating rely on the assumption that the nonlinear state of these plasma instabilities efficiently convert the kinetic energy of the beam and convert it into heat. In our previous work, we appealed to nonlinear simulations conducted in a radically different regime to argue for such a conversion. However, a full nonlinear study is called for. We begin this task in this initial work where we study the distribution function of the electron-positron pairs that are produced from VHEGR-EBL photon annihilation. We study the evolution of a distribution function under Lorentz transformations to develop an analytic understanding of how the perpendicular and parallel velocity dispersions transform under boosts. Using this understanding, we then develop a simple description of the distribution function of the beam, which we then use to calculate the unstable modes analytically in both the reactive (hydrodynamic) and kinetic regimes. Here the reactive instability refers to the instability where the entire beam participates in the instability. In particular, all the beam particles are resonant with the unstable wave on a timescale longer than the growth time of the instability. The reactive instability is also referred to as the hydrodynamic instability since the instability can be derived from the fluid equations instead of kinetic theory. On the other hand, in the kinetic regime, only a fraction of the beam particles are resonant with the beam over a the growth time of the instability, which reduces the growth rate compared to the reactive instability for the same beam density and beam Lorentz factor. We recover the well-known results for the reactive regime for both the beam-plasma and "oblique" modes. We also derive the growth rate for these two instabilities in the kinetic regime and delineate the range of applicability for both the reactive and kinetic cases and apply these results for ultrarelativistic e^+e^- pair beams.

This paper is organized as follows. In Section 2, we describe the transformation properties of an ultrarelativistic e^+e^-

---

[2] In order to follow the plasma literature more closely, henceforth we will refer to what we have called the "two-stream" instability as the "beam-plasma" instability

beam in terms of its distribution function. We then calculate the various linear instabilities that this beam is subject to in section 3. In particular, we pay careful attention to both the reactive (or hydrodynamic) and kinetic regimes of the beam plasma and "oblique" instabilities and the transition between the two. Applying these result to TeV electron-positron pair beams that arise from TeV photon pair production in Section 4, we demonstrate the despite the extraordinary coldness of the beam that we are always in the kinetic regime for the "oblique" mode, but may be in the reactive regime for the beam plasma mode. However, because the controlling parameter is close to unity, the growth rates calculated in either regime are similar. We close with a discussion the implications of this work and application of these results for nonlinear theory in Section 5.

2. ULTRARELATIVISTIC PAIR BEAMS FROM VHEGRS

As stated in the Introduction, VHEGR photons pair produce on encountering EBL photons as they propagate throughout the universe (Gould & Schréder 1966), and this attenuation of VHEGR flux has been use as a probe of the EBL (Stecker et al. 1992; de Jager et al. 1994; Aharonian et al. 2006). The basic requirement of this process is that the energies of the VHEGR (E_{ph}) and the EBL photon (E_{ebl}) exceed the rest mass energy of the $e^{\pm}$ pair in the center of momentum (COM) frame, i.e., $2EE_{ebl}(1 - \cos\theta) \geq 4m_e^2 c^4$, where θ is the relative angle of propagation in the lab frame, an $e^{\pm}$ pair can be produced with Lorentz factor $\gamma \simeq E/2m_e c^2$ (Gould & Schréder 1967a). Here, we discuss the distribution function of the pair beam that emerges from this process.

2.1. Distribution Function of the Pair Beam

In the COM frame of the beam, we assume that the distribution function is isotropic, such that $f = f(E)$ is just a function of energy. We model this distribution as a relativistic thermal distribution:

$$f \propto \exp\left(-\frac{E}{T}\right), \qquad (1)$$

where E and T are the dimensionless energy and temperature in terms of a particles rest mass. In the non-relativistic case, this reduces to the Maxwell-Boltzmann distribution, while the relativistic version is known as the Maxwell-Juttner distribution (**REFS**).

The relativistic Maxwellian distribution can be extended to a drifting (or boosted) distribution via an appropriate Lorentz transformation. The relationship between the energies of the lab (boosted) frame and the COM frame is (Jackson)

$$E_{CM} = \gamma_B \left(E_L - \beta_B p_{L,\parallel} \right). \qquad (2)$$

Plugging this into (1), we find (Wright & Hadley 1975)

$$f = \frac{n_b m_e c^2}{4\pi \gamma_B k_B T K_2(m_e c^2/k_B T) m_e^3 c^3} \exp\left(-\frac{\gamma_B(E - \mathbf{v}_B \cdot \mathbf{p})}{k_B T}\right) \quad (3)$$

where K_2 is the 2nd order modified Bessel function. The transformation properties of the drifting Maxwell-Juttner distribution coupled with the Lorentz invariance of the distribution function (as discussed in Appendix **??**) demonstrates that the drifting Maxwell-Juttner distribution is the correct description of a boosted isotropic Maxwellian (relativistic or otherwise).

3. LINEAR THEORY

The Vlasov equation for each species is

$$\frac{\partial f_s}{\partial t} + \mathbf{v}_s \cdot \nabla f_s + q_s \left(\mathbf{E} + \frac{\mathbf{v}_s}{c} \times \mathbf{B} \right) \cdot \nabla_p f_s = 0, \qquad (4)$$

where $\mathbf{v}_s = \mathbf{p}_s/\gamma_s m_e$ and $\gamma_s = 1/\sqrt{1 - v_s^2/c^2}$ Here, s is the species label, $+$ for positrons and $-$ for electrons, with $q_{\pm} = \pm e$. Upon linearizing this in small perturbations about a background distribution, i.e., setting $f_s \to f_{0s} + \delta f_s$, $\mathbf{B} \to \delta \mathbf{B}$ and $\mathbf{E} \to \delta \mathbf{E}$, we obtain,

$$\frac{\partial \delta f_s}{\partial t} + \mathbf{v}_s \cdot \nabla \delta f_s + q_s \left(\delta \mathbf{E} + \frac{\mathbf{v}_s}{c} \times \delta \mathbf{B} \right) \cdot \nabla_p f_{0s} = 0. \quad (5)$$

The plasma couples to the field through the Maxwell equations

$$\nabla \times \delta \mathbf{E} = -\frac{1}{c} \frac{\partial \delta \mathbf{B}}{\partial t}, \qquad (6)$$

$$\nabla \times \delta \mathbf{B} = \frac{4\pi}{c} \delta \mathbf{j} + \frac{1}{c} \frac{\partial \delta \mathbf{E}}{\partial t}, \qquad (7)$$

where $\delta \mathbf{j} = \sum_s q_s \int \mathbf{v}_s \delta f_s d^3 p$ is the linear current density perturbation.

Here it is useful to work within the electrostatic approximation ($\mathbf{k} \times \delta \mathbf{E} = 0$), where we only need to include Coulomb's law for the electric field rather than the full Maxwell equations:

$$i\mathbf{k} \cdot \delta \mathbf{E} = 4\pi \delta \rho, \qquad (8)$$

where $\delta \rho = \sum_s q_s \int \delta f_s d^3 p$ is the perturbed charge density. By adopting the electrostatic approximation, we have explicitly ignored electromagnetic modes. This would preclude, for example, the Weibel instability. In addition, the electromagnetic terms would introduce corrections to the physics that are not necessarily small in the limit of relativistic particles, i.e., $v/c \to 1$. However, we make this approximation for two reasons. First, a complete calculation of the unstable modes has already been carried out by Bret et al. (2010), who showed that the electrostatic approximation is in excellent agreement with a full calculation (modulo the Weibel instability). Second, the electrostatic approximation is much simpler than a full calculation and allows us to analytically calculate the unstable growth rates, while permitting a clear exposition of the relevant physics.

We now adopt perturbations of the form $\delta \sim \exp(i\mathbf{k} \cdot \mathbf{r} - i\omega t)$ and without loss of generality assume that $\mathbf{k} = (k_x, 0, k_z)$, where k_z is along the beam direction. Linearizing the Vlasov-Maxwell equations then leads to the dispersion relation:

$$\epsilon = 1 + \sum_s \frac{m_e \omega_{p,s}^2}{k^2} \int \frac{\mathbf{k} \cdot \nabla_p F_s}{\omega - \mathbf{k} \cdot \mathbf{v}} d^3 p = 0, \qquad (9)$$

where ϵ is the simplified dielectric function, and for each species $\omega_{p,s}^2 \equiv 4\pi e^2 n_s/m_e$ is the plasma frequency, $n_s \equiv \int f_{0s} d^3 p$ is the number density, and $F_s \equiv f_{0s}/n_s$ is the normalized distribution function. Upon integrating by parts, Equation (9) becomes

$$\epsilon = 1 - \sum_s \frac{m_e \omega_{p,s}^2}{k^2} \int F_s \mathbf{k} \cdot \nabla_p \frac{1}{\omega - \mathbf{k} \cdot \mathbf{v}} d^3 p$$

$$= 1 - \sum_s \frac{\omega_{p,s}^2}{k^2 c^2} \int F_s \frac{k^2 c^2 - (\mathbf{k} \cdot \mathbf{v})^2}{\gamma(\omega - \mathbf{k} \cdot \mathbf{v})^2} d^3 p = 0. \quad (10)$$

There are two distinct, often qualitatively different, regimes in which we may consider the implications of this dispersion

relation. The first is the cold plasma limit or the hydrodynamic or reactive limit. The hydrodynamic limit is aptly named because the resulting dispersion relation that is found could have also been calculated directly from the continuity equation and the momentum equation. In this limit, the internal distribution of the particles of the background or beam are irrelevant to the physics of the instability and it is only the bulk response that is important. In particular, this means that the beam particles are resonance with the unstable wave over a timescale much longer than the growth them as stated above, i.e., the beam particles do not drift a distance larger than the wavelength of the unstable mode over the growth time of the instability. The second is the kinetic regime, where the internal distribution of the beam particles are important to the physics of the instability. Here, only a fraction of the beam particles stay within one wavelength of the unstable mode over the growth time of the instability. Here, the bulk of the plasma (background or beam) do not response to the disturbance, but rather only a fraction of the particles are relevant for driving (instability) or damping (Landau damping). We discuss below the evaluation of the dispersion relation in these two regimes, which gives two regimes of instability, and the delineation between these two regimes.

3.1. Hydrodynamic (Reactive) Instability

Starting with the dispersion relation (10), we first consider the instability of a cold plasma beam. Taking the limit of Equation (3) as $\alpha_\parallel^{-1}, \alpha_\perp^{-1} \to 0$, for a target plasma $v_0 = 0$ and a beam plasma $v_0 = v_b$[3], we find

$$1 - \frac{\omega_{p,t}^2}{\omega^2} - \frac{\omega_{p,b}^2}{\gamma^3(\omega - k_z v_b)^2} \frac{\gamma^2 k_x^2 + k_z^2}{k_x^2 + k_z^2} = 0. \quad (11)$$

For $k_x = 0$, we recover the same beam-plasma instability which was described in the Appendix of Broderick et al. (2012).

The solution to Equation (11) is given in Appendix A where we show that the associated growth rate (eq.[A4]) is

$$\Gamma = \frac{\sqrt{3}}{2^{4/3}} \left(\frac{n_b}{n_t}\right)^{1/3} \left(\frac{\gamma^2 Z_x^2 + 1}{Z_x^2 + 1}\right)^{1/3} \frac{\omega_{p,t}}{\gamma}, \quad (12)$$

where $Z_x = k_x v_b / \omega_{p,t}$ is the dimensionless wavevector perpendicular to the beam direction.

For $k_x = 0 \to Z_x = 0$, this reduces to the beam-plasma growth rate, which is

$$\Gamma = \Gamma_{TS} \equiv \frac{\sqrt{3}}{2^{4/3}} \left(\frac{n_b}{n_t}\right)^{1/3} \frac{\omega_{p,t}}{\gamma}, \quad (13)$$

which we denote the beam-plasma or "two-stream" growth rate. For the more general case where $Z_x \neq 0$, this becomes the oblique instability studied by Bret et al. Indeed for $\gamma \gg 1$ and $Z_x \sim 1$, the growth rate approaches oblique growth rate:

$$\Gamma = \Gamma_{ob} \equiv \frac{\sqrt{3}}{2^{4/3}} \left(\frac{n_b}{n_t}\right)^{1/3} \frac{\omega_{p,t}}{\gamma^{1/3}}, \quad (14)$$

which is much faster than the beam-plasma growth rate, Γ_{TS}.

We should caution in the derivation above that the resonance condition, which is $\omega_{p,t} - k_z v_b$, implies that $k_z \neq 0$. For the case where $k_z \to 0$, the electrostatic approximation no longer holds and the full dispersion relation must be solved.[4] A solution to

___

[3] That is, we set $F_s(\mathbf{p}) = \delta^3(\mathbf{p} - \mathbf{p}_{0s})$ where $\mathbf{p}_{0s} \equiv \gamma_0 m_e v_0 \hat{\mathbf{z}}$ is the momentum associated with v_0.

[4] We thank Antoine Bret for helping to clarify this point.

the full dispersion relation reveals additional modes, including the zero frequency ($k_z = 0$) filamentation or Weibel mode.

3.2. Kinetic Instability

The growth rate expressed in Equation (12) sits in the reactive (or hydrodynamic) regime as the dispersion relation (Equation (A1)) could be been derived from the fluid equations. Here all the particles participate in the instability. However, kinetic theory masks another regime of the instability, where only a fraction of the particle participate in the instability, i.e., the kinetic regime. We now derive the growth rate of the instability in the kinetic regime.

We begin first with the distribution function for the target plasma:

$$F_t = \left(\frac{1}{2\pi m_e k_B T}\right)^{3/2} \exp\left(-\frac{p^2}{2m_e k_B T}\right), \quad (15)$$

where the target plasma is assumed to be nonrelativistic, $\mathbf{p} = m_e \mathbf{v}$ is the nonrelativistic momentum, and T is the temperature of the background. For the beam plasma, we adopt the Maxwell-Juttner distribution (eq.[3]). Plugging these into the dispersion relation (9), we find

$$1 - \frac{\omega_{p,t}^2}{k^2 c^2} \int F_t \frac{k^2 c^2 - (\mathbf{k} \cdot \mathbf{v})^2}{\gamma(\omega - \mathbf{k} \cdot \mathbf{v})^2} d^3 p + \frac{m_e \omega_{p,b}^2}{k^2} \int \frac{\mathbf{k} \cdot \nabla_p F_b}{\omega - \mathbf{k} \cdot \mathbf{v}} d^3 p = 0, \quad (16)$$

where we have integrated by parts only the second term, associated with target plasma.

We discuss the solution to Equation (16) in Appendix B. The associate growth rate for the kinetic beam plasma instability is

$$\Gamma \simeq -\Gamma_0 \frac{\pi \gamma_w^2 \gamma_{ph}^3 m(v_{ph} - v_{B,z'})}{4\gamma_b \mu K_2(\mu) \mathcal{G}'^3} \left[(\mathcal{G}'^2 \mu^2 + 2\mathcal{G}' \mu + 2) + \frac{\gamma_B^2 v_{B,x'}^2}{2\mathcal{G}^2 c^2}(2\mathcal{G}' \mu + 2)\right] \text{ex} \quad (17)$$

where $\Gamma_0 \equiv \omega_p \gamma_B (n_b/n_t)(m_e v_B^2/k_B T)$ is the typical maximum growth rate.

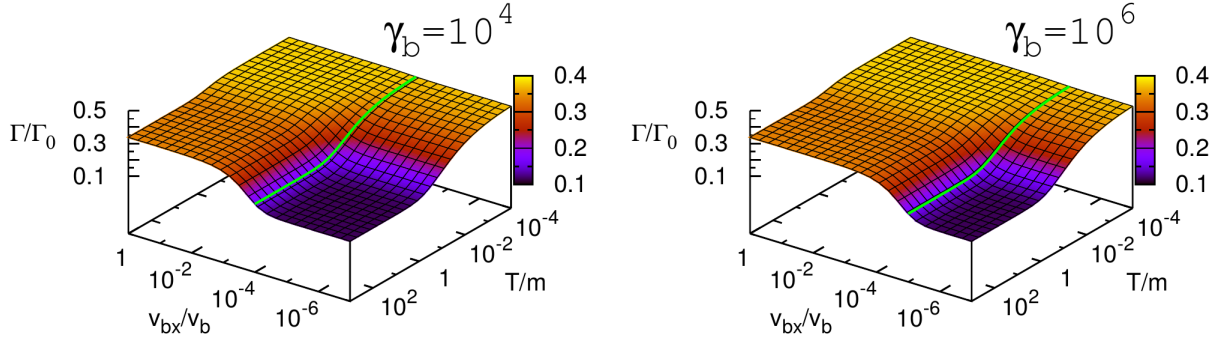In Figure 1, we plot the maximum growth rate (maximized over v_{ph}) as function of $v_{bx} = |k_{bx} v_b/k|$ and T. From the figure, it is clear that the growth rate is maximized for $v_{bx}/v_b \gg 1/\gamma_b$. Moreover the maximum growth rates vary little and are robust for broad range of $v_{bx}/v_b = k_{bx}/k$, i.e., large range in angles between beam and wavevector. Hence, this suggests that we might estimate the maximal oblique growth rates by taking the limit as $v_{bx} \gg v_b/\gamma_b$ and maximizing over v_{ph}. This is further seen in Figure 2, we maximize over both v_{bx} and v_{ph}. Here for relativistic beams, the maximum growth rate varies little with T, varying by less than 10% between hot and cold beams. Thus, we find:

$$\Gamma_M \simeq \begin{cases} 0.38\Gamma_0 & k_B T/m_e c^2 \ll 1 \\ 0.34\Gamma_0 & k_B T/m_e c^2 \gg 1 \end{cases}, \quad (18)$$

for $\gamma_b \gtrsim 10$, as seen in Figure 2.

3.3. The Transition between the Kinetic and Hydrodynamic Instability

The oblique instability exists in two different regimes, raising the important question: how are the two regimes related to each other. While this question has been studied by many authors in the context of the beam-plasma or two-stream instability (see for instance Melrose 1986; Boyd & Sanderson 2003),

Figure 1. Oblique growth rate maximized over v_{ph} as a function of v_{bx} and T for various γ_b. In each the green line shows the chord along which $v_{bx}/v_b = 1/\gamma_b$. In all cases, the maximum growth rate occurs when $v_{bx}/v_b \gg 1/\gamma_b$.
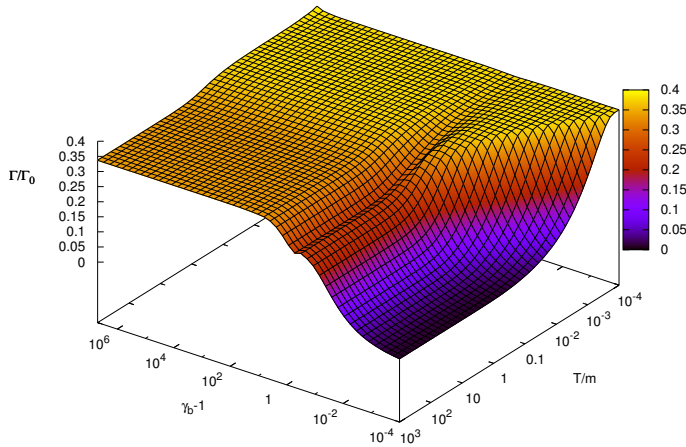
Figure 2. Oblique kinetic growth rate, maximized over v_{bx}/v_b and ω/k, normalized by $\Gamma_0 \equiv \omega_{Pt}(n_b/n_t)\gamma_b m v_b^2/T$ as a function of T (in units of m) and γ_b. Note that unlike the beam plasma case shown in Figure **??**, at high γ_b the transition between high and low temperature is only marginal, constituting a roughly 10% reduction.

a clear exposition of how these two regimes are related to each other is lacking.

To begin let us return to the reactive instability. For the growth rate of the reactive instability (12) to be valid, the velocity dispersion $\to 0$. To reach this limit, we demand

$$\mathbf{k} \cdot \Delta\mathbf{v} \ll \omega - \mathbf{k} \cdot \mathbf{v}_b. \tag{19}$$

Taking $\mathbf{k}$ to be $\omega_{p,t}/v_b$, so that the RHS is $\approx \Gamma$, we find

$$\frac{\Delta v_\perp}{v_b} \ll \left(\frac{n_b}{\gamma_b n_t}\right)^{1/3} \tag{20}$$

where we have dropped constant factors of order unity and assumed that $Z_x \sim O(1)$. Hence, this defines the upper limit on the velocity dispersion of the plasma for the cold-plasma approximation to hold and, hence, the range of validity for the reactive oblique growth rate (12). For $Z_x \ll \gamma^{-2}$, we recover the condition for the relativistic, reactive beam-plasma instability (Boyd & Sanderson 2003)

$$\frac{\Delta v_\parallel}{v_b} \ll \gamma_b^{-1} \left(\frac{n_b}{n_t}\right)^{1/3}. \tag{21}$$

Applying these results to the case of ultrarelativistic beams

and given our results from Section 2, we find

$$\frac{\Delta v_\perp}{v_b} \sim \sqrt{\alpha_\perp} = \sqrt{\alpha'_\perp}\gamma^{-1}, \tag{22}$$

$$\frac{\Delta v_\parallel}{v_b} \sim \sqrt{\alpha_\parallel} = \sqrt{\alpha'_\parallel}\gamma^{-2}, \tag{23}$$

where $\alpha'_\perp$ and $\alpha'_\parallel$ encodes the dependence on the COM velocity dispersion. Hence, the conditions for the reactive regime for the "oblique" mode (eq.[20]) and beam-plasma mode (eq.[21]) can be reduced to

$$1 \ll \begin{cases} \alpha_\perp'^{-1/2}\gamma_b^{2/3}\left(n_b/n_t\right)^{1/3} & \text{"oblique"} \\ \alpha_\parallel'^{-1/2}\gamma_b\left(n_b/n_t\right)^{1/3} & \text{beam plasma} \end{cases}. \tag{24}$$

We now proceed to study the range of validity for the kinetic growth rate for the beam plasma mode (eq.[**??**]) and "oblique" mode (eq.[**??**]). Following the argument of Boyd & Sanderson (2003), the growth occurs over a range where the distribution function is positive or $v_b - \Delta v < \omega/k < v_b$. Hence the bandwidth over which the distribution powers grows is $\Delta\omega \sim k\Delta v$ For the beam plasma case, the growth rate is roughly

$$\Gamma \sim \frac{n_b}{\gamma^3 n_t}\left(\frac{c}{\Delta v_\parallel}\right)^2. \tag{25}$$

The bandwidth, $\Delta\omega$, is then greater than the growth rate if

$$\frac{\Delta v_\parallel}{v_b} \gtrsim \gamma^{-1}\left(\frac{n_b}{n_t}\right)^{1/3}, \tag{26}$$

which connects with the condition on the reactive beam plasma instability from Equation (21). Similarly for the "oblique" mode, the bandwidth, $\Delta\omega$, is then greater than the growth rate if

$$\frac{\Delta v_\perp}{v_b} \gtrsim \left(\frac{n_b}{\gamma n_t}\right)^{1/3}, \tag{27}$$

which can similarly compared to the condition on the reactive "oblique" mode from Equation (20).

Combining these two kinetic condition and our result again from Section 2, we find

$$1 \geq \begin{cases} \alpha_\perp'^{-1/2}\gamma_b^{2/3}\left(n_b/n_t\right)^{1/3} & \text{"oblique"} \\ \alpha_\parallel'^{-1/2}\gamma_b\left(n_b/n_t\right)^{1/3} & \text{beam plasma} \end{cases}, \tag{28}$$

which in combination with Equation (24) denotes the transition between the reactive and kinetic regimes.

4. APPLICATION TO ULTRARELATIVISTIC e^+e^- BEAMS

As discussed in the Introduction, the annihilation of VHE-GRs and EBL photons produce ultrarelativistic e^+e^- beams that are unstable to the beam plasma and "oblique" modes discussed above. To apply the above results to the ultrarelativistic e^+e^- beams, we now calculate their initial conditions.

4.1. Average COM Energy of the e^+e^- Beam

To find the effective velocity dispersion of the ultrarelativistic e^+e^- beam, we must first estimate the average COM energy of the beam. To do so, we consider the process of photon-photon annihilation. For a monoenergetic population of VHEGR photons with energy E_{ph}, the production rate of e^+e^- on EBL photons is

$$\Gamma_\pm(E_{ph}) = \int \sigma c \, dn_{ebl}$$
$$= \int \sigma\left(E_{ph}, E_{ebl}\right) c \frac{dn_{ebl}}{dE_{ebl}} dE_{ebl}, \qquad (29)$$

where $\Gamma_\pm$ is the rate of pair production, σ is the pair-production cross section, n_{ebl} is the number density of EBL photons, and E_{ebl} is the energy of the EBL photons. There are two important components to this calculation – the cross section, σ, and the spectra of the EBL.

For σ, we use the results from Nikishov (1962) and Gould & Schréder (1967b), who considered a high energy photon with energy E_{ph} moving along the x-axis annihilating on an EBL photon with energy E_{ebl} moving at an angle, θ, with respect to the x-axis. The total cross section for this process is (Nikishov 1962; Gould & Schréder 1967b)

$$\sigma = \frac{1}{2}\pi r_e^2 \left(1 - \frac{v_e^2}{c^2}\right)\left[\left(3 - (v_e/c)^4\right)\ln\frac{1 + v_e/c}{1 - v_e/c} - 2\frac{v_e}{c}\left(2 - \frac{v_e^2}{c^2}\right)\right], \qquad (30)$$

where $r_e = e^2/m_e c^2$ is the classical electron radius and v_e is the electron velocity in the COM frame. To find v_e, we use the energy of the electron in the COM frame, E_e, which is

$$E_e = \frac{m_e c^2}{\sqrt{1 - v_e^2/c^2}} = \sqrt{\frac{1}{2}E_{ebl}E_{ph}(1 - \cos\theta)}. \qquad (31)$$

Pair production occurs when $E_e/m_e c^2 \geq 1$.

The second ingredient is the spectra of the EBL, which is not well constrained. Here we use the constraints from Aharonian et al. (2006), who demonstrated that VHEGR emission from H 2356-309 and 1ES 1101-232 places an upper limit on the EBL that is close to the lower limit of the integrated light from galaxies Madau & Pozzetti (2000). Looking at Figure 1 of Aharonian et al. (2006), we note that the EBL has a flat spectrum, i.e., constant dn_{ebl}/dE_{ebl} below 1 eV and a falling spectrum $dn_{ebl}/dE_{ebl} \propto E_{ebl}^{-1.5}$ with a spectral index of ≈ 1.5 above 1 eV with a rapid cutoff above 10 eV. Thus, we adopt a simplified model:

$$\frac{dn_{ebl}}{dE_{ebl}} \propto \begin{cases} E_{ebl}^0 & E_{ebl} \leq 1\,\text{eV} \\ E_{ebl}^{-1.5} & 1\,\text{eV} < E_{ebl} \leq 10\,\text{eV} \\ 0 & E_{ebl} > 10\,\text{eV} \end{cases} \qquad (32)$$

In Figure 3, we plot the differential rate of pair production as a function of the COM energy of the electron (and positron)
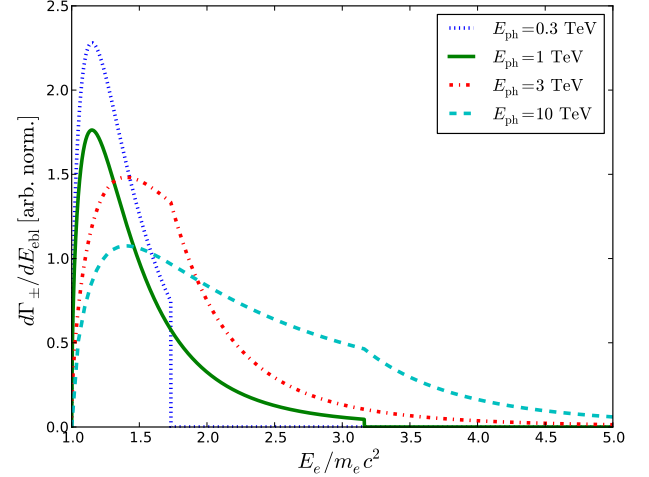
Figure 3. Differential rate of pair production as a function of the COM energy of the electron (and positron) for a photon energy of $E_{ph} = 0.3$ (dotted line), 1 (solid line), 3 (dash-dotted line) and 10 TeV (dashed line). The effect of the EBL spectra can be seen in different features in this plot. The cutoff in $d\Gamma_\pm/dE_{ebl}$ above $E_e/m_e c^2 \approx 3$ for $E_{ph} = 1$ TeV is due to the cutoff in the EBL spectra above 10 eV. The break in $d\Gamma_\pm/dE_{ebl}$ at the same position for $E_{ph} = 10$ TeV is due to change in the EBL spectra at 1 eV. The average COM energies of the produced electrons are $E_e/m_e c^2 \approx 1.3, 1.6, 2$, and 3 for $E_{ph} = 0.3, 1, 3$, and 10 TeV, respectively.

for a photon energy of $E_{ph} = 0.3$ (dotted line), 1 (solid line), 3 (dash-dotted line) and 10 TeV (dashed line). We use the COM energy in this case because in the COM frame, the energy of the EBL and TeV photon is the same and is $E_{CM} = \sqrt{E_{ebl}E_{ph}}$ and $\theta \approx \pi - \sqrt{E_{ebl}/E_{ph}} \to \cos\theta = -1$, allowing us to ignore the dependence on θ in Equation (30). We note several feature of this Figure. First the distribution of COM energy for the electrons (and positrons) depends on the initial photon energy. This is because different energy photons probe different regimes of the EBL spectra. Due to the rapid cutoff in the EBL above 10 eV, lower energy VHEGRs produce colder beams. This is seen in the average COM energies of the produced electrons, which are respectively, $E_e/m_e c^2 \approx 1.3, 1.6, 2$ and 3 for $E_{ph} = 0.3, 1, 3$ and 10 TeV. Hence we expect that these pairs are in the sub-relativistic to mildly-relativistic regimes in their COM frame. Second, the effect of the EBL spectra on the distribution of electron COM energies is also seen in the breaks in the distribution. For instance, the cutoff in $d\Gamma_\pm/dE_{ebl}$ above $E_e/m_e c^2 \approx 3$ for $E_{ph} = 1$ TeV is due to the cutoff in the EBL spectra above 10 eV. Additionally, the break in $d\Gamma_\pm/dE_{ebl}$ at the same position for $E_{ph} = 10$ TeV is due to change in the EBL spectra at 1 eV.

4.2. Regime of Instability

Given that the range of $E_e/m_e c^2$ between $1.3 - 3$ for $E_{ph} = 1 - 10$ TeV, this corresponds to values of $\alpha'_\perp$ and $\alpha'_\parallel$ between $\sim 0.3 - 2$. To determine whether or not the reactive or kinetic instabilities apply to these beams, it is necessary to determine n_b/n_t. Here the target is the background IGM, so $n_t = n_{IGM}$, where $n_{IGM} \approx 2 \times 10^{-7}(1 + \delta)(1 + z)^3\,\text{cm}^{-3}$ is the mean density of the IGM, z is the redshift, and δ denotes the overdensity. The number density of the TeV beam is more complicated as the production rate of pairs must be balanced against their loss due to plasma instabilities or ICC. This is discussed extensively in Paper I and will not be repeated here. However, we note that the

important issue here is the loss rate due to plasma instabilities, which is a nonlinear process. In Paper I, we assumed that the nonlinear loss rate was the same as the linear growth rate. This remains to be shown and is the focus of ongoing work, of which this paper lays the initial foundation.

Still some progress can be made if we assume that the dominant loss rate is ICC so that we can place a lower limit on the various plasma processes. In this case, the ratio of the beam plasma density to the IGM, n_b/n_{IGM}, is then (Paper I):

$$\frac{n_b}{n_{IGM}} \simeq \frac{L_E}{2\pi D_{pp}^3 \Gamma_{IC}} \frac{1}{n_{IGM}}$$

$$\simeq 3 \times 10^{-18} \left(\frac{1+z}{1}\right)^{3\zeta-7} \left(\frac{EL_E}{10^{45} \mathrm{erg\,s^{-1}}}\right) \left(\frac{E}{\mathrm{TeV}}\right) \mathrm{cm}^{-3} \quad (33)$$

where D_{pp} is defined in the Introduction to be the mean free path of a VHEGR, L_E is the isotropic luminosity of the VHEGR source, E is the energy of the VHEGR photon, Γ_{IC} is the inverse Compton cooling rate, and ζ is.

In Section 3.3, we derived the controlling parameter that delineates the reactive (eq.[24]) and kinetic regimes (eq.[28]) by comparing the frequency spread of resonant waves, $\Delta\omega \sim k\Delta v$, with the growth rate, Γ. Applying these conditions (eqns. [24] and [28]) to the ultrarelativistic e^+e^- pair beams of interest, we find for the controlling parameter:

$$\frac{\gamma_b^{2/3}}{\sqrt{\alpha'_\perp}} \left(\frac{n_b}{n_{IGM}}\right)^{1/3} = 7 \times 10^{-3} \frac{\gamma_6^{2/3}}{\sqrt{\alpha'_\perp}} (1+z)^{\zeta-7/3}$$
$$\left(\frac{EL_E}{10^{45} \mathrm{erg\,s^{-1}}}\right)^{1/3} \left(\frac{E}{\mathrm{TeV}}\right)^{1/3}, \quad (34)$$

and

$$\frac{\gamma_b}{\sqrt{\alpha'_\parallel}} \left(\frac{n_b}{n_{IGM}}\right)^{1/3} = 0.7 \frac{\gamma_6}{\sqrt{\alpha'_\parallel}} (1+z)^{\zeta-7/3}$$
$$\left(\frac{EL_E}{10^{45} \mathrm{erg\,s^{-1}}}\right)^{1/3} \left(\frac{E}{\mathrm{TeV}}\right)^{1/3}, \quad (35)$$

where $\gamma_6 = \gamma/10^6$. We see from our reactive (24) and kinetic (28) conditions, that the "oblique" instability always exists in the kinetic regime, but the beam plasma instability can also sit in the reactive regime for sufficiently cold beams $\alpha_\parallel \lesssim 0.5$, which occurs $E_{ph} \sim 1\,\mathrm{TeV}$ and for large γ, which occurs for $E_{ph} \sim 10\,\mathrm{TeV}$.

The discussion above confirmed our earlier estimate in Paper I that the "oblique" instability sits in the kinetic regime. However, our new results suggest that the beam-plasma instability matches the "oblique" instability in effective growth rate in the kinetic regime and that the beam-plasma mode may also sit in the reactive regime. However, we do not expect that the reactive beam-plasma mode will have a major effect on our earlier results. First, plasma instabilities losses on the TeV pairs could easily push the beam plasma mode into the kinetic regime by reducing n_b, but this requires a proper estimate of the effect of the nonlinear instability. This is a part of ongoing work and will be presented in a future publication. Second, while it seems that the beam plasma mode may sit in the reactive regime, it is not too far from the kinetic regime, i.e., the controlling parameter, $(\gamma_b/\sqrt{\alpha'_\parallel})(n_b/n_{IGM})^{1/3}$, is order unity. Thus, both the reactive and the kinetic growth rates are similar and likely

makes little difference for the beam plasma mode which regime is assumed (in terms of growth rate). Therefore, the use of the kinetic growth rate for the "oblique" mode (and beam-plasma mode) in Paper I is valid, and the results of this paper buttresses the results of Paper I, II, III, and Puchwein et al. (2012).

5. SUMMARY AND CONCLUSION

The ultrarelativistic e^+e^- beams that result from VHEGR-EBL annihilation are subject to powerful plasma beam instabilities including the beam plasma and "oblique" instability. In this work, we have these linear instabilities as they would apply to the ultrarelativistic pair beams. Our main findings are:

- We calculate how the parallel and perpendicular velocity dispersions of a distribution function responds under Lorentz boosts. We show that these two velocities dispersions respectively scale like γ^{-2} and γ^{-1}, allowing us to develop a simplified distribution function of the TeV electron-positron beam. We also show that this can be identified with a drifting relativistic Maxwell-Juttner distribution.

- Using this simplified distribution function, we have analytically calculated the beam-plasma and "oblique" instabilities in both the reactive and kinetic regime. We have recovered the reactive scalings for the beam-plasma mode $\Gamma \sim \gamma^{-1}(n_b/n_t)^{1/3}$ and the "oblique" mode $\Gamma \sim (n_b/\gamma n_t)^{1/3}$. In the kinetic regime, we have shown that the growth rate for both modes have the same scaling and similar normalization.

- We have also delineated the regime of applicability of the kinetic and reactive calculation and found, while the kinetic growth rates are similar for both the beam plasma and "oblique" mode, the condition for transition between the kinetic and reactive regimes for both are different. In particular, the beam-plasma mode transitions at a lower value of γ in comparison to the "oblique" mode. This is due to a difference of $\gamma^{1/3}$ scaling between the two modes.

- We calculate the average COM energy of the ultrarelativistic pair beam using a simplified model of the spectra of the EBL. We found that the average energy of these beams range from $E_e/m_e c^2 = 1.3-3$ for $E_{ph} = 1-10\,\mathrm{TeV}$, with colder beams at lower energies. This is due to the rapid cutoff in the EBL above 10 eV.

- Using this average COM energy, we presume that the pair beam can be modelled as a relativistic Maxwellian in the COM frame. We then demonstrate that the "oblique" mode is in the kinetic regime. However, the beam plasma mode is marginally in the reactive regime, so that the use of either regime produces roughly the same growth rate. Moreover, the inclusion of plasma instability losses on the number density of beam particles may place the beam plasma mode firmly in the kinetic regime.

The results of this paper are a first step toward an understanding of the nonlinear regime of these plasma instabilities for ultrarelativistic e^+e^- beams. In particular, by developing a simple distribution function, whose modes can be analytically calculated, we will develop a quasilinear theory for these modes in

a forthcoming publication. Such a quasilinear calculation will capture the dominant wave-particle interaction and capture the initial nonlinear evolution of this instability.

APPENDIX

A. SOLUTION FOR THE REACTIVE REGIME

This can be rewritten as

$$\left(\omega^2 - \omega_{p,t}^2\right)\left[(\omega - k_z v_b)^2 - \frac{\omega_{p,b}^2}{\gamma^3}\frac{\gamma^2 k_x^2 + k_z^2}{k_x^2 + k_z^2}\right] = \frac{\omega_{p,t}^2 \omega_{p,b}^2}{\gamma^3}\frac{\gamma^2 k_x^2 + k_z^2}{k_x^2 + k_z^2} \quad (A1)$$

where we have added a factor of $\gamma^{-3}\omega_{p,t}^2\omega_{p,b}^2(\gamma^2 k_x^2 + k_z^2)/(k_x^2 + k_z^2)$ to both sides. To solve the dispersion relation (A1), we take $\omega = \omega_{p,t} + \Delta\omega$ and expand to lowest order in $\Delta\omega$ and $\omega_{p,b}$. This gives

$$2\Delta\omega\omega_{p,t}\left(\Delta\omega + \omega_{p,t} - k_z v_b\right)^2 = \frac{\omega_{p,t}^2 \omega_{p,b}^2}{\gamma^3}\frac{\gamma^2 k_x^2 + k_z^2}{k_x^2 + k_z^2}. \quad (A2)$$

For $\Delta\omega \ll \omega_{p,t} - k_z v_b$, $\Delta\omega$ is real and there is no instability. However, if $k_z = \omega_{p,t}/v_b$, we then have

$$\Delta\omega^3 = \omega_{p,t}^3 \frac{\omega_{p,b}^2}{2\gamma^3\omega_{p,t}^2}\frac{\gamma^2 Z_x^2 + 1}{Z_x^2 + 1}, \quad (A3)$$

where we have multiplied the fraction on the right hand side by $(v_b/\omega_{p,b})^2/(v_b/\omega_{p,t})^2$ and $Z_x = k_x v_b/\omega_{p,t}$ is the dimensionless wavevector perpendicular to the beam direction. Equation (A3) gives three solutions for $\Delta\omega$: one real and two imaginary (one growing and one damping). The maximum growth rate is then

$$\Gamma = \frac{\sqrt{3}}{2^{4/3}}\left(\frac{n_b}{n_t}\right)^{1/3}\left(\frac{\gamma^2 Z_x^2 + 1}{Z_x^2 + 1}\right)^{1/3}\frac{\omega_{p,t}}{\gamma} \quad (A4)$$

B. SOLUTION FOR THE KINETIC REGIME

As the target plasma is nonrelativistic, we can take $v \ll c$ and $\gamma \to 1$. Expanding the denominator in powers of v, we find

$$\int F_t \frac{k^2 c^2 - (\mathbf{k}\cdot\mathbf{v})^2}{\gamma(\omega - \mathbf{k}\cdot\mathbf{v})^2}d^3p \approx k^2 c^2 \int F_t\left(\frac{1}{\omega^2} + \frac{2\mathbf{k}\cdot\mathbf{v}}{\omega^3} + \frac{3(\mathbf{k}\cdot\mathbf{v})^2}{\omega^4}\right)d^3p$$

$$\approx \frac{k^2 c^2}{\omega^2}\left(1 + 3k^2\lambda_D^2\right), \quad (B1)$$

where the second term is zero because it is odd, **$\lambda_D^2 = k_B T/m_e\omega_p^2$ is the Debye length, and we have assumed that $k^2\lambda_D^2 \ll 1$ and $\omega \approx \omega_p$ in the last term on the RHS**[5]. If we ignore the third term in the kinetic dispersion relation (16),

---

[5] A direct solution to equation (B1) without approximating $\omega \approx \omega_p$ will reveal waves with nontrivial growth or damping rates. These wave are not legitimate and result from the Taylor expansion of the denominator of equation (B1). A correct treatment of equation (B1) with the appropriate Landau contours will give the correct growing or damping behaviors for waves with phase speeds approximately that of the electron phase speeds.

this yields two plasma modes: an undamped plasma oscillation mode with $\omega = \omega_{p,t}$ and a longitudinal electron plasma wave, i.e., Langmuir wave, with

$$\omega = \omega_{p,t}\left(1 + \frac{3}{2}k^2\lambda_{D,t}^2\right). \quad (B2)$$

To compute the contribution from the beam term, we will reorient our coordinate system and define the z'-axis along the wavevector, $\mathbf{k}$. In this case we have the beam taking on a non-z' component, $\mathbf{v}_b = v_{bz'}\hat{\mathbf{z}}' + v_{bx}\hat{\mathbf{x}}'$. This frame moves with a velocity, $\mathbf{v}_{ph} = \omega_k/k\hat{\mathbf{z}}'$. With an eye toward computing the residue in (??), we define $p_{z'} = \gamma_{z'}v_{z'}\epsilon_\perp$, $\epsilon = \gamma_{z'}\epsilon_\perp$, and $\epsilon_\perp = \sqrt{m^2 + p_\perp^2}$ is the perpendicular energy. In this case, we can rewrite the beam distribution function as

$$F_B = \frac{m_e c^2}{4\pi\gamma_B k_B T K_2(m_e c^2/k_B T)m_e^3 c^3}\exp\left(-\frac{\gamma_B(E - v_{B,z'}p_{z'} - v_{B,x'}p_{x'})}{k_B T}\right) \quad (B3)$$

$$= \frac{\mu m_e^{-3}c^{-3}}{4\pi\gamma_B K_2(\mu)}\exp\left(-\frac{\gamma_B\gamma_{z'}(c^2 - v_{B,z'}v_{z'})\epsilon_\perp}{k_B T c^2}\right)\exp\left(\frac{\gamma_B v_{B,x'}p_{x'}}{k_B T}\right) \quad (B4)$$

Plugging the equation into (??), we find that the this gives an associated growth rate of

$$\Gamma \simeq -\omega_p\frac{\pi n_b}{2n_t}m_e v_B^2 R, \quad (B5)$$

which involves the integral of

$$R \equiv \int \frac{k\partial F_b/\partial p_{z'}}{\omega - k_{z'}v_{bz'}}d^3p, \quad (B6)$$

where R is the residue for $p_{z'}$ such that $v_{z'} = v_{ph}$. Here we find for the two elements that contribute to the pole:

$$\frac{\partial}{\partial p_{z'}}(\omega - kv_{bz'})\bigg|_{pole} = -k\left(\frac{c^2}{\epsilon} - \frac{p_{z'}^2 c^4}{\epsilon^3}\right)\bigg|_{pole} = -\frac{kc^2}{\gamma_{ph}^3\epsilon_\perp}, \quad (B7)$$

and

$$k\frac{\partial F_b}{\partial p_{z'}}\bigg|_{pole} = -\frac{k\gamma_B}{k_B T}\left(\frac{p_{z'}c^2}{\epsilon} - v_{B,z'}\right)F_b\bigg|_{pole}$$

$$= -\frac{k(v_{ph} - v_{B,z'})\mu m_e^{-3}c^{-3}}{4\pi k_B T K_2(\mu)}\exp\left(-\frac{\gamma_B\gamma_{ph}(c^2 - v_{B,z'}v_{ph})\epsilon_\perp}{k_B T c^2}\right)$$

$$\exp\left(\frac{\gamma_B v_{B,x'}p_{x'}}{k_B T}\right). \quad (B8)$$

Putting this all together, the residue is

$$R = \frac{\gamma_{ph}^3(v_{ph} - v_{B,z'})\mu}{4\pi k_B T K_2(\mu)}\frac{\mathcal{I}}{m_e^3 c^5}, \quad (B9)$$

where

$$\mathcal{I} \equiv \int d^2 p_\perp \epsilon_\perp \exp\left(-\frac{\mathcal{G}(\epsilon_\perp - wp_x)}{k_B T}\right) \quad (B10)$$

and $\mathcal{G} \equiv \gamma_B\gamma_{ph}(1 - v_{B,z'}v_{ph}/c^2)$ and $w \equiv \gamma_B v_{B,x'}/\mathcal{G} \leq 1$. This latter inequality is guaranteed as

$$\mathcal{G}\epsilon_\perp - \gamma_B v_{B,x'}p_{x'} = \gamma_B(E - v_{B,z'}p_{z'} - v_{B,x'}p_{x'})|_{v_{B,z'}=v_{ph}} > 0 \quad (B11)$$

is the energy in beam frame and is therefore positive definite. Noting that the $\exp(-wp_{x'})$ term appears as a boosted distribution, we boost by w along the x'-axis, removing the anisotropic term from the exponential.

Thus, we define $p'_{x'} = \gamma_w(p_{x'} - w\epsilon_\perp)$ and $p'_{y'} = p_{y'}$ and find:

$$\epsilon_\perp = \gamma_w(\epsilon'_\perp + wp'_x), \quad (B12)$$

$$dp_x dp_y = \frac{\epsilon_\perp}{\epsilon'_\perp} dp'_x dp'_y. \quad (B13)$$

Inserting this into equation (B9), we find

$$
\begin{aligned}
\mathcal{I} &= \int d^2 p'_\perp \frac{\epsilon^2_\perp}{\epsilon'_\perp} \exp\left(-\frac{\mathcal{G}'\epsilon'_\perp}{k_B T}\right) \\
&= \pi\gamma_w^2 \int_0^\infty dp'^2_\perp \left(\epsilon'_\perp + \frac{w^2}{2}\frac{p'^2_\perp}{\epsilon'_\perp}\right) \exp\left(-\frac{\mathcal{G}'\epsilon'_\perp}{k_B T}\right),
\end{aligned} \quad (B14)
$$

where $\mathcal{G}' \equiv \mathcal{G}/\gamma_w$. Note in the second line that we have used isotropy in $\mathbf{p}'_\perp$ to eliminate terms linear in $\mathbf{p}'_\perp$. Using the following integrals:

$$\int_0^\infty dx\sqrt{1+x}\, e^{-a\sqrt{1+x}} = \frac{2e^{-a}}{a^3}\left(a^2 + 2a + 2\right) \quad (B15)$$

and

$$\int_0^\infty dx \frac{x}{\sqrt{1+x}} e^{-a\sqrt{1+x}} = \frac{4(a+1)}{a^3} e^{-a}, \quad (B16)$$

we find

$$\mathcal{I} = \frac{2\pi\gamma_w^2 m_e^3 c^4}{\mathcal{G}'^3\mu^3}\left[\left(\mathcal{G}'^2\mu^2 + 2\mathcal{G}'\mu + 2\right) + \frac{w^2}{2c^2}\left(2\mathcal{G}'\mu + 2\right)\right]\exp\left(-\mathcal{G}'\mu\right). \quad (B17)$$

Inserting this into (B8) yields

$$R = \frac{\gamma_{\rm ph}^3\gamma_w^2(\nu_{\rm ph} - \nu_{B,z'})}{2\mu m_e c^2 \mathcal{G}'^3 K_2(\mu)}\left[\left(\mathcal{G}'^2\mu^2 + 2\mathcal{G}'\mu + 2\right) + \frac{\gamma_B^2 \nu_{B,x'}^2}{2\mathcal{G}^2 c^2}\left(2\mathcal{G}'\mu + 2\right)\right]\exp\left(-\mathcal{G}'\mu\right) \quad (B18)$$

and therefore,

$$\Gamma \simeq -\Gamma_0 \frac{\pi\gamma_w^2\gamma_{\rm ph}^3 m(\nu_{\rm ph} - \nu_{B,z'})}{4\gamma_b\mu K_2(\mu)\mathcal{G}'^3}\left[\left(\mathcal{G}'^2\mu^2 + 2\mathcal{G}'\mu + 2\right) + \frac{\gamma_B^2 \nu_{B,x'}^2}{2\mathcal{G}^2 c^2}\left(2\mathcal{G}'\mu + 2\right)\right]\exp\left(-\mathcal{G}'\mu\right) \quad (B19)$$

where $\Gamma_0 \equiv \omega_p\gamma_B(n_b/n_t)(m_e\nu_B^2/k_B T)$ is the typical maximum growth rate.

REFERENCES

Aharonian, F., et al. 2006, Nature, 440, 1018

Bolton, J. S., & Becker, G. D. 2009, MNRAS, 398, L26
Boyd, T. J. M., & Sanderson, J. J. 2003, The Physics of Plasmas, ed. Boyd, T. J. M. & Sanderson, J. J.
Bret, A., Firpo, M., & Deutsch, C. 2004, Phys. Rev. E, 70, 046401
Bret, A., Gremillet, L., & Bénisti, D. 2010, Phys. Rev. E, 81, 036402
Broderick, A. E., Chang, P., & Pfrommer, C. 2012, ApJ, 752, 22
Chang, P., Broderick, A. E., & Pfrommer, C. 2012, ApJ, 752, 23
de Cea del Pozo, E., Torres, D. F., & Rodriguez Marrero, A. Y. 2009, ApJ, 698, 1054
de Jager, O. C., Stecker, F. W., & Salamon, M. H. 1994, Nature, 369, 294
Dermer, C. D., Cavadini, M., Razzaque, S., Finke, J. D., Chiang, J., & Lott, B. 2011, ApJ, 733, L21
Dolag, K., Kachelriess, M., Ostapchenko, S., & Tomàs, R. 2011, ApJ, 727, L4
Domingo-Santamaría, E., & Torres, D. F. 2005, A&A, 444, 403
Faucher-Giguère, C., Lidz, A., Zaldarriaga, M., & Hernquist, L. 2009, ApJ, 703, 1416
Ghisellini, G., & Maraschi, L. 1989, ApJ, 340, 181
Ghisellini, G., Maraschi, L., & Tavecchio, F. 2009, MNRAS, 396, L105
Ghisellini, G., & Tavecchio, F. 2008, MNRAS, 387, 1669
Gould, R. J., & Schréder, G. 1966, Physical Review Letters, 16, 252
Gould, R. J., & Schréder, G. P. 1967a, Physical Review, 155, 1408
—. 1967b, Physical Review, 155, 1404
Inoue, Y., & Totani, T. 2009, ApJ, 702, 523
Jones, T. W., O'dell, S. L., & Stein, W. A. 1974, ApJ, 192, 261
Kneiske, T. M., & Mannheim, K. 2008, A&A, 479, 41
Kravtsov, A. 2010, Advances in Astronomy, 2010
Lacki, B. C., Thompson, T. A., Quataert, E., Loeb, A., & Waxman, E. 2011, ApJ, 734, 107
Madau, P., & Pozzetti, L. 2000, MNRAS, 312, L9
McQuinn, M., Lidz, A., Zaldarriaga, M., Hernquist, L., Hopkins, P. F., Dutta, S., & Faucher-Giguère, C. 2009, ApJ, 694, 842
Melrose, D. B. 1986, Instabilities in Space and Laboratory Plasmas, ed. Melrose, D. B.
Narumoto, T., & Totani, T. 2006, ApJ, 643, 81
Neronov, A., & Vovk, I. 2010, Science, 328, 73
Nikishov, A. I. 1962, JETP, 14, 393
Paglione, T. A. D., Marscher, A. P., Jackson, J. M., & Bertsch, D. L. 1996, ApJ, 460, 295
Peebles, P. J. E. 2001, ApJ, 557, 495
Persic, M., Rephaeli, Y., & Arieli, Y. 2008, A&A, 486, 143
Pfrommer, C., Chang, P., & Broderick, A. E. 2012, ApJ, 752, 24
Puchwein, E., Pfrommer, C., Springel, V., Broderick, A. E., & Chang, P. 2012, MNRAS, 423, 149
Rephaeli, Y., Arieli, Y., & Persic, M. 2010, MNRAS, 401, 473
Stecker, F. W., de Jager, O. C., & Salamon, M. H. 1992, ApJ, 390, L49
Takahashi, K., Mori, M., Ichiki, K., & Inoue, S. 2012, ApJ, 744, L7
Tavecchio, F., & Ghisellini, G. 2008, MNRAS, 386, 945
Tavecchio, F., Ghisellini, G., Bonnoli, G., & Foschini, L. 2011, MNRAS, 414, 3566
Tavecchio, F., Ghisellini, G., Foschini, L., Bonnoli, G., Ghirlanda, G., & Coppi, P. 2010, MNRAS, 406, L70
Taylor, A. M., Vovk, I., & Neronov, A. 2011, A&A, 529, A144
Thompson, T. A., Quataert, E., & Waxman, E. 2007, ApJ, 654, 219
Venters, T. M. 2010, ApJ, 710, 1530
Viel, M., Bolton, J. S., & Haehnelt, M. G. 2009, MNRAS, 399, L39
Vovk, I., Taylor, A. M., Semikoz, D., & Neronov, A. 2012, ApJ, 747, L14